THE UNIVERSITY OF SYDNEY
SCHOOL OF MATHEMATICS AND STATISTICS

MATH3888 – GROUP 9

Characterisation of the behaviour of the Connor-Stevens (CS) model for neurons, with reference to physical data

Albert Stark:	540657726	Calvin Ming En Kok:	530263092
Kyle George:	520417425	Tim Lin:	530532035

Contents

1 Introduction

We aim to analyse the Connor-Stevens (CS) model [3] for neural excitability in Python and XPPAUT. The CS model allows one to analyse and predict the behaviour of a Potassium (K), Sodium (Na), mixed Potassium/Sodium and leaky channel via an extension of the well known Hodgkin-Huxley model. Our analysis includes time trace and eigenvalue analysis with comparison to a known dataset, as well as the use of a, to our knowledge, novel methodology for bifurcation analysis of this large-dimensional model, which has been implemented in Python.

1.1 Biological Setting

A neuron is a cell that forms part of the neural system of a living organism. Such cells exhibit excitability in their behaviour, the modeling of which is desirable for physiologists, but also for medicine and wider biology. Each of these cells have a number of ion channels, the output of which is experimentally observable, and can be assigned an "openness" value $t \in [0, 1]$ with 0 being completely closed, and 1 being completely open. The responds to the presence of certain chemicals, known as "neurotransmitters", and will release an electrical signal in response to a high enough presence of such chemicals and the openness of the cells ion channels will vary with this electrical signal. Conversely, the cell may be stimulated with an electrical signal, and the effects on various channels can then be observed.

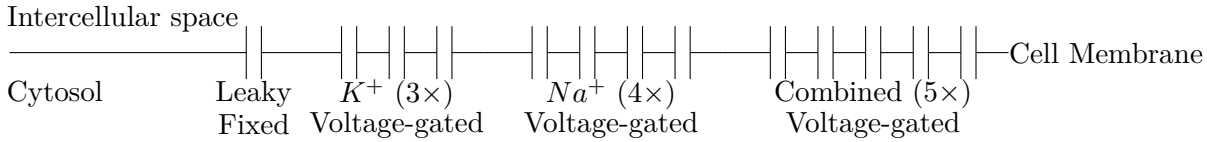

Figure 1: Diagram of the cell membrane and channels

2 Agonists and Drugs

In our experiments, we simulated the action of standard pharmacological tools by changing CS model parameters (conductances and, where relevant, kinetics). Below, each drug is introduced with its established biophysical action and our corresponding simulation hypothesis.

Tetrodotoxin (TTX) — voltage-gated Na^+ channel blocker. TTX occludes the pore of voltage-gated sodium channels, abolishing action-potential initiation and propagation.
Simulation mapping: set the fast sodium conductance to zero ($\overline{g}_3 \to 0$).
Hypothesis: removing I_{Na} suppresses repetitive spiking and leaves the membrane at or near rest, with only subthreshold dynamics driven by leak and K^+ currents.

4-Aminopyridine (4-AP) — blocker. Blocks the transient A-type K^+ current I_A.
Simulation mapping: reduce or disable A-type conductance ($\overline{g}_4 \downarrow$ or $= 0$).
Hypothesis: lower threshold/latency, increased firing; onset shifts toward Type-II/Hopf-like regimes.

Tetraethylammonium (TEA) — delayed-rectifier K^+ channel blocker. TEA is a pore blocker of many voltage-gated K^+ channels, including delayed rectifiers; its interaction with K^+ channels was established electrophysiologically and later rationalized structurally [1, 6, 5].
Simulation mapping: we mimicked TEA by reducing $\overline{g}_2$ (delayed-rectifier I_K).
Hypothesis: weakening I_K broadens spikes and slows repolarization; at stronger block it can promote irregular firing under current injection.

Drug	Primary target	CS parameterization	Expected effect
TTX	Nav pore block	$\overline{g}_3 \to 0$	Abolish spiking; rest dominates
4-AP	I_A (A-type K^+) block	$\overline{g}_4 \downarrow /0$	Lower threshold; higher rate
TEA	Delayed-rectifier K^+ block	$\overline{g}_2 \downarrow$	Broader spikes; slower V reset

3 Experimental Protocol

The dataset that we are comparing against is for the Giant Squid and is from the work of Paydafar and others [8]. The methodology for how this data set was obtained can be found in the accompanying paper [7]. We compared the results of our model to this data throughout. For discussion of the specifics of our model implementation see the section on our mathematical modelling. Having received results from this model we would attempt to verify the behaviour predicted from our implemented model with the dataset, which we discuss below. Additionally, we studied the system in XPPAUT and also compared this output to that of our model.

Discoveries of various bifurcations (LPs, a codimentsion 3 Pitchfork) were found in our Python program, and other bifurcations (AH, LPOC for saddle-node, and a suspected potentially a period-doubling point) were found in XPPAUT. Where possible these were cross-checked with our Python model and with physiological data [8] where possible.

4 Mathematical Modelling

4.1 The Connor-Stevens model

The Connor-Stevens (CS) ion channel model depicts a series of ion channels, with different behaviours over an index $j \in \{1, 2, 3, 4\}$ corresponding to K^+ $(j = 2), Na^+$, $(j = 3)$ a leaky channel $(j = 1)$ and a combined K^+ and Na^+ channel $(j = 4)$. The a variables correspond to the proportion of open channels and b variables are the closed channels.

$$I(t) = C_m \frac{dv}{dt} + \sum_{j=1}^{4} \overline{g}_j (A_j(V,t))^j B_j(V,t)(V - V_j) \tag{1}$$

The numerical assignment j directly corresponds to the quantity of each channel in a complete set within in the cell. Each channel over j has its own representative A_j and B_j functions:

$$\tau_{Aj}(V)\frac{dA_j(V,t)}{dt} + A_j(V,t) = A_j(V,\infty)$$
$$\tau_{Bj}(V)\frac{dB_j(V,t)}{dt} + B_j(V,t) = B_j(V,\infty)$$

which are in turn dependent on time constant $\tau(V)$ functions and their steady states at infinite time $A_j(V,\infty)$ and $B_j(V,\infty)$. The $\tau(V)$ time constants control the response rate of each channel's throughput, where a high value describes a slow reaction to a voltage change. To simplify the problem, we elected to remove the voltage dependence of the leaky channel, reducing nine variables to seven. This is also an unusual feature of this model compared to the others. Table 1 gives the types of each function and the associated parameters we can use for bifurcation analysis are in Table 2.

5 Modelling results

5.1 Findings

5.1.1 Fast–timescale subsystem (V, a_3, a_4, b_3): bifurcation in I_{app}

Model/solver. We use the Connor–Stevens conductance form (n^4, m^3h, a^3b) with voltage–dependent $x_\infty(V)$ and $\tau_x(V)$ fits, integrated by Gear/BDF (`dt`=0.05, `toler`=10^{-7}). Continuation in I_{app} is done in XPPAUT/AUTO with HB/LP detections; plotting follows the standard legend: red/black (stable/unstable equilibria), green/blue (stable/unstable cycles).

Key findings. (i) Rest→spiking via Hopf: As I_{app} increases, the stable equilibrium loses stability at an HB near $I_{\text{app}} \approx 8.8$, producing a small-amplitude stable limit cycle whose amplitude and period grow with current (tonic spiking). (ii) Finite stability window for the LC: The green branch persists over an intermediate current range; near its ends AUTO shows a stability change to blue, consistent with secondary bifurcation/mesh limits. The reported period at a marked point is ≈ 163 ms, consistent with partial availability of I_A during ISIs. (iii) Artifact note: A blue arc near $I_{\text{app}} \approx 7.518$ is contradicted by local Jacobian eigenvalues $\{-2.156\times10^{-3}, -8.333\times10^{-2}, -1, -0.2\}$ (all negative), so we treat it as a continuation/initialization artifact; AUTO documentation recommends refining mesh/steps and checking multipliers in such cases.

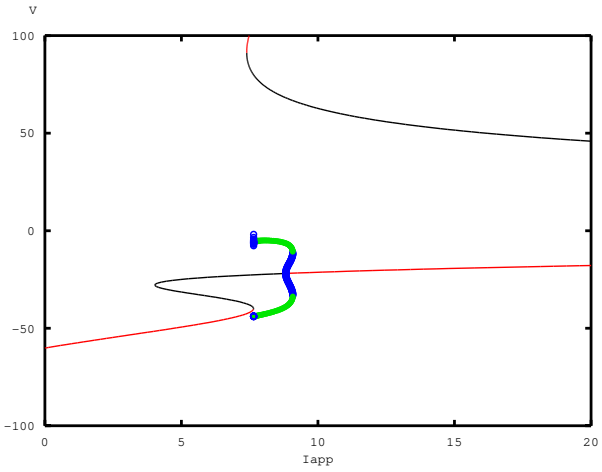

Figure 2: **Fast subsystem vs. I_{app}.** V (mV) vs. I_{app}. Red=stable eq., black=unstable eq.; green=stable LC (extrema of V), blue=unstable LC. A supercritical Hopf gives the tonic-spiking branch.

5.1.2 Middle–timescale subsystem (QSS-fast): (V, b_2, b_3) continuation in I_{app}

Model/solver. Fast gates ($n \sim a_2$, $m \sim a_3$, $a \sim a_4$) were treated by a quasi–steady-state (QSS) reduction, i.e. $x = x_\infty(V)$, leaving (V, b_2, b_3) dynamic. Kinetics follow Connor–Stevens; continuation in I_{app} used XPPAUT/AUTO with HB/LP detection and standard stability coloring (red/black equilibria; green/blue cycles).

Key findings. (i) S-shaped equilibria with folds (bistability): The equilibrium curve is S-shaped with two turning points (folds/saddle–nodes), yielding a finite window of input-driven bistability (coexistence of a depolarized and a hyperpolarized fixed point). (ii) No Hopf bifurcation

in this slice: Under QSS-fast, we did not detect a Hopf bifurcation, nor stable limit cycles across the scanned I_{app} range; treating the fast activations as instantaneous removes the mechanism that seeds small-amplitude oscillations near the original Hopf point in the fast system. (iii) Interpretation: This reduction captures the static I–V nonlinearity (folds/bistability) while suppressing fast regenerative dynamics; it is consistent with singular-perturbation/QSS heuristics (fast gates slaved to V).

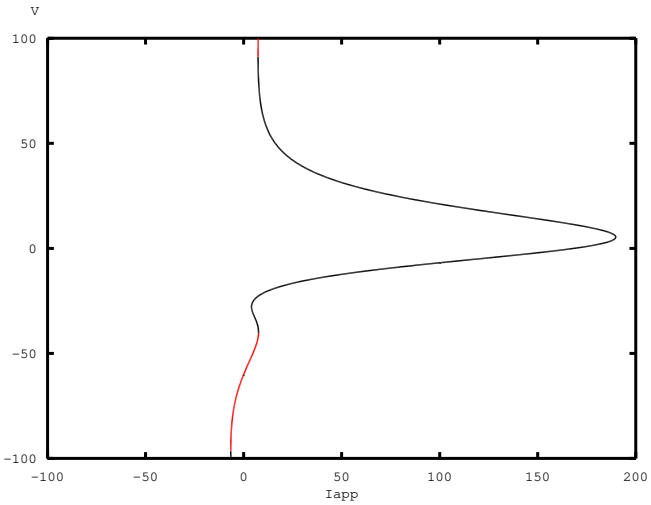

Figure 3: **Middle (QSS-fast) subsystem vs. I_{app}.** V (mV) versus I_{app}. Red: stable equilibria; black: unstable equilibria. No sustained periodic orbits are detected in this slice over the scanned range.

5.1.3 Slow–timescale subsystem: (V, a_2, b_2, b_3, b_4) vs. I_{app}

Model/solver. From the full CS model we retain the slow gates (a_2, b_2, b_3, b_4) as dynamic and treat the fast activations a_3, a_4 in QSS ($a_3 = a_{3,\infty}(V)$, $a_4 = a_{4,\infty}(V)$). Continuation in I_{app} is done in XPPAUT/AUTO with the same color legend: red/black (stable/unstable equilibria), green/blue (stable/unstable cycles).

Key findings. (i) Rest→spiking via Hopf: A Hopf bifurcation occurs at $(I_{\text{app}}, V) \approx (27.7, -16.04)$, where the equilibrium loses stability and a small-amplitude limit cycle is born (blue near HB). (ii)Unstable blue arc at the left edge: Sampling an equilibrium near the dense blue region gave eigenvalues $\{+0.002081, -0.006689, -0.020826, -0.020000, -0.200000\}$, i.e., one positive real part ⇒ **unstable** (index-1 saddle), consistent with the blue labeling there. (iii) Overlap segment check: On the portion where green and blue dots visually overlap, direct eigenvalue checks at nearby equilibria were **negative** (stable). We therefore interpret the blue markers in that narrow overlap as plotting/continuation artifacts; the underlying state is stable (matching the green classification). (iv) Blue near HB is correct: The blue cycle close to the Hopf point remains **unstable**, as expected for the small nascent orbit immediately after HB in this slice.

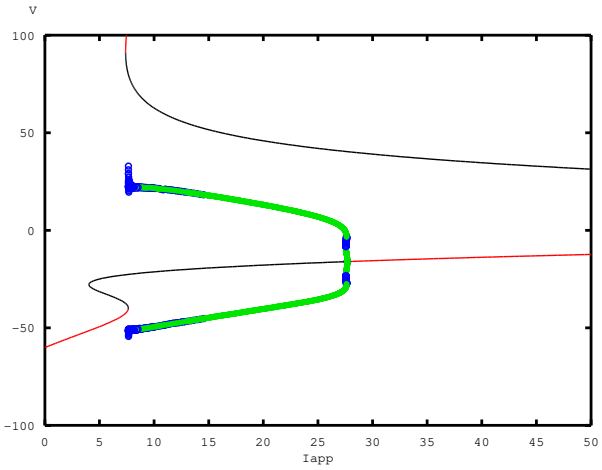

Figure 4: **Slow subsystem vs. I_{app}.** V (mV) against I_{app}. Red=stable eq., black=unstable eq.; green=stable LC, blue=unstable LC. HB marks the Hopf point.

5.1.4 Tools

We used QSS reduction for fast gates in the middle and slow system and XPPAUT/AUTO continuation with eigenvalue and cycles checks for stability. Also used XPPAUT/AUTO for the bifurcation diagrams

5.2 Full System Time Traces

We produced time trace plots for the system with Python within the Andronov-Hopf bifurcation limit cycle region, shown in Figure 5. By changing V_4, the combined channel Nernst potential, the system entered and exited this region, stopping and then restarting the oscillations. Oscillations affect every variable, however the a variables spike in the opposite direction to the b variables. a_4 and b_4 produce sawtooth wave-like oscillations.

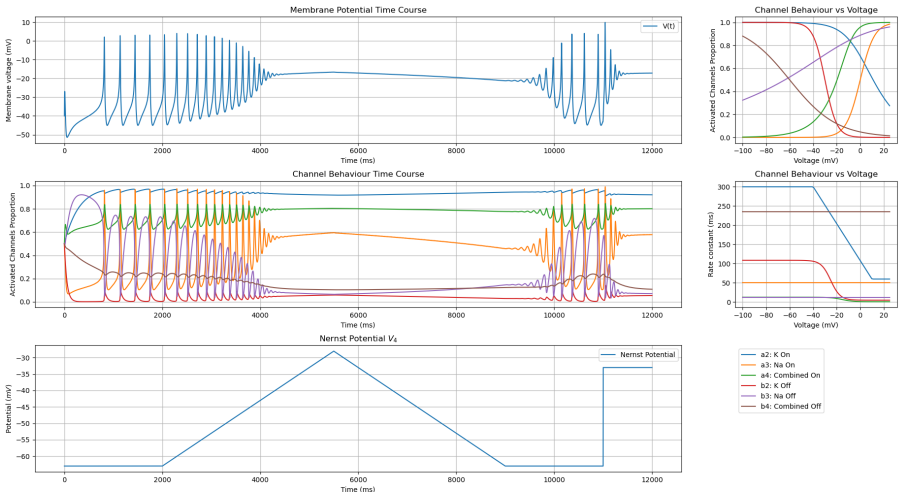

Figure 5: Time trace under a slowly varying V_4 and $I_{\text{app}} = 10\mu\text{A}$.

5.2.1 Full System Phase Plots

Under the same circumstances as the time traces, we produced phase plots of the Hopf bifurcation. Figure 6 shows the resulting plot, for $V(t)$ and b_4 as changes to V_4 affect a_4 and b_4 most.

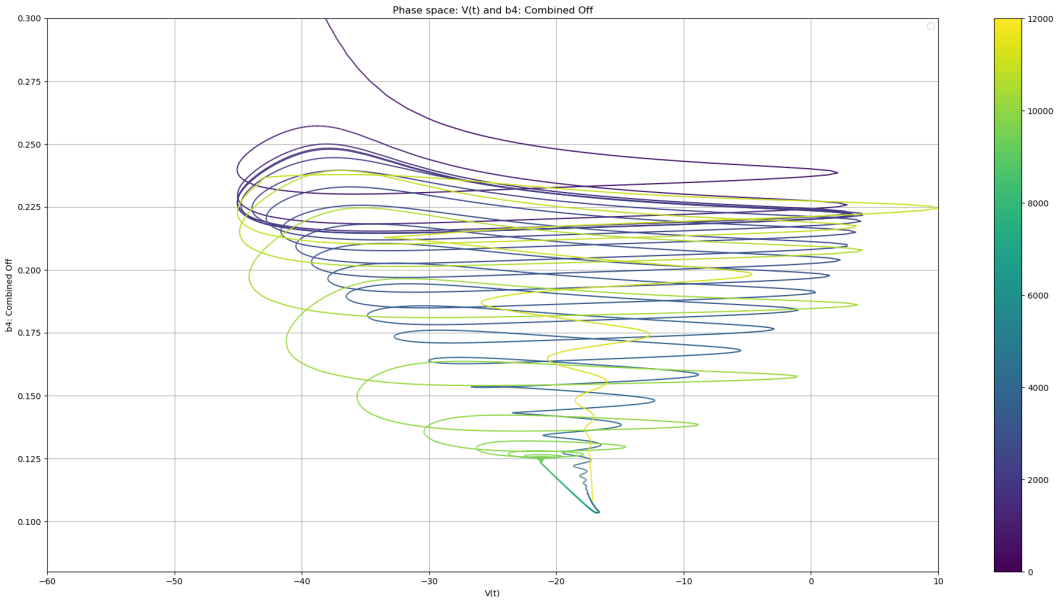

Figure 6: Phase plot in $V(t)$ vs b_4 of the system over time, with time displayed by the colours on the right.

5.2.2 Full System Pitchfork Bifurcation

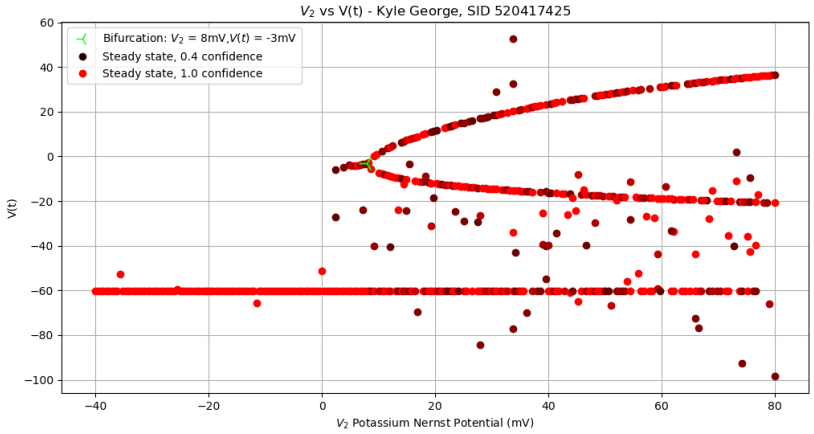

Figure 7: Full system supercritical pitchfork bifurcation at $V_2 \approx 8\text{mV}, V \approx -3\text{mV}$.

Using Python for our bifurcation analysis of the full system, we found a supercritical pitchfork bifurcation in the parameter V_2, Potassium Nernst potential, as seen in Figure 7. Therefore, an increase in V_2 creates two stable steady states in addition to the line of stable states across the bottom of Figure 7. Please see the appendix for plots in other variables. The other variables exhibit a similar pattern, giving coordinates of the pitchfork at $(v_2, v_3) = (8, -45)$ and $(v, a_2, a_3, a_4, b_2, b_3, b_4) = (-3, 0.76, 0.92, 0.87, 0.36, 0.005, 0.055)$. From the perspective of

the equations, there are pitchfork bifurcations in V_2, V_3, V_4 as Equation 1 is odd in terms of V. Tracking this further, we also found a codimension 3 pitchfork bifurcation for $(V_2, V_3, V_4) = (11.0, 0.00, -42)$, $(v, a_2, a_3, a_4, b_2, b_3, b_4) = (-10, 0.8, 0.9, 0.9, 0.2, 0.1, 0.1)$, which was found using Python. This point has three separate lines of pitchfork bifurcations intersecting and none proceed past (in this case, V_2, V_4 decreasing and V_3 increasing) the point. We searched comprehensively over V_2 and V_3, then inferring the V_4 component by checking above and below the bifurcation in V_2 and V_3. This reduced the computation time to nine hours, as compared to searching all parameters explicitly.

5.2.3 Full System Andronov–Hopf Bifurcation

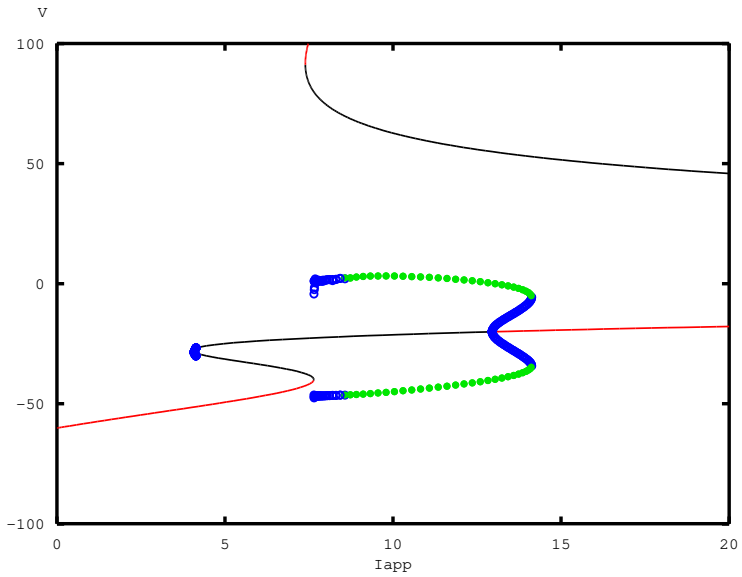

Figure 8: Full CS system, exhibiting an Andronov-Hopf Bifurcation (Artifact at Iapp=8

Using XPPAUT we found an Andronov-Hopf bifurcation in the applied current, shown in Figure 8. This occurs at $I_{app} \approx 12.95$mA. This supports the Andronov-Hopf bifurcations found in the slow and fast subsystems. The unstable oscillations near $I_{app} \approx 4.082$ do exist but ended up not producing any oscillations in our model.

5.3 Modelling tools

The CS model presents two difficulties to the standard methods of numerical continuation. First, as a seven-dimensional system, it is difficult to visualise the behaviours and steady states in all seven variables are more difficult to find. Starting guesses for solvers become more difficult to decide on. Second, the convergence rates of most numerical solvers are very low on this model due to the time constants τ being large, the sigmoidal functions and numerous powers and roots. As a result, we developed a novel method of bifurcation analysis. To find steady states, we begin a standard algorithm at a random point, and repeat enough times to attain a clear result, usually ten thousand times or more. Any results that exceed physicality cutoffs (voltages more than 500mV and ratios outside $[0, 1]$) are removed, then the remaining results are sorted

depending on the Euclidean distance to the centre of each group of points. These clusters are then the required steady states. A per-cluster confidence is also created as the ratio between the quantity of results in the current cluster and the highest count of results in any cluster. To represent this, Figure 7 has red dots to mark high confidence and black ones for low confidence. Then, as usual, the eigenvalues are computed for each steady state and plotted against the parameter. There are a maximum of seven eigenvalues, so the bifurcations are flagged when any of them cross the imaginary axis (real part zero).

6 Interpretation and Discussion

The results that we have obtained from our model align with the expected behaviour of a neuron insofar as they can model oscillatory behaviour. Additionally, there is further physiological significance that can be lent to the codimension 3 pitchfork bifurcation that was found. Specifically, given that the Nernst Potential V_2 follows $V_2 \propto \log \frac{[K^+]_{\text{in}}}{[K^+]_{\text{out}}}$ at equilibrium, a drop in Nernst potential corresponds to an increase in the external ion concentration. V_3 uses Na^+ and acts similarly, while V_4, as a combined channel, acts on the weighted sum $A[K^+] + B[Na^+]$, depending on how many of each ion is moved in or out. This is caused by neuronal swelling, such as during a TBI (Traumatic Brain Injury) or inundation of neurotransmitters such as in epileptic events. Our model then gives plausability to the potential effectiveness of electrical stimulation as a treatment for TBI or epilepsy. This is borne out by further research in both TBI [9] and epilepsy [2] treatments, and provides a mathematical basis for these treatments.

Additionally, we attempted to find agreement between our model and the dataset of Payadafar [7][8]. This work was done on Giant Squid axons, and was characterising the behaviour of those cells with reference to the Hodgkin-Huxely model [4]. Unfortunately we were unable to replicate the results of the dataset. This is because of the strong interdependence between the variables of our particular model meaning that they cannot be isolated to act as a bistable switch, and so the change in behaviour as demonstrated by Payadafar [7] from milisecond-length pulses cannot be represented. The code can potentially be modified further to allow for this modelling to occur but would have to occur as part of further research into this topic. We also may have some constant parameters in our governing functions that could be non-physical. See appendix A.2 for the parameters that we used throughout. Some of these values were taken directly from [3], but others such as the power sigmoidal type functions, and those for the non-constant τ functions had to have their values interpolated. Further experimentation is required to obtain accurate values for these parameters.

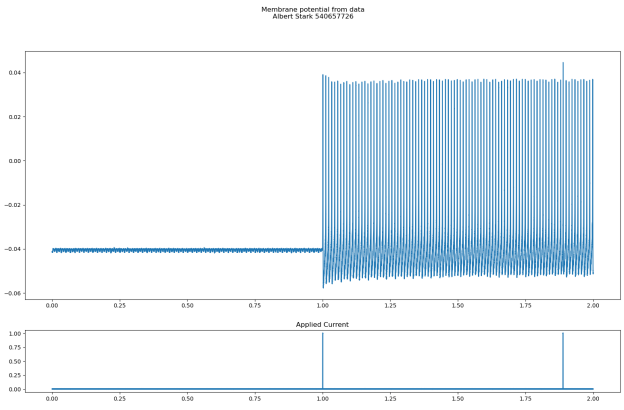

Time trace of data from sample a1t18 of Payadafar[8], the top trace is membrane voltage, the bottom trace is applied current

References

[1] Clay M. Armstrong. **?**Interaction of Tetraethylammonium Ion Derivatives with the Potassium Channels of Giant Axons**?** **in***Journal of General Physiology*: 58.4 (1971), **pages** 413–437. DOI: 10.1085/jgp.58.4.413.

[2] Y Chen **andothers**. **?**Transcranial direct current stimulation in the management of epilepsy: a meta-analysis and systematic review**?** **in***Frontiers in Neurology*: (2024). DOI: 10.3389/fneur.2024.1462364.

[3] John A. Connor **and** Charles F. Stevens. **?**Prediction of repetitive firing behaviour from voltage-clamp data on an isolated neurone soma**?** **in***The Journal of Physiology*: 213.1 (1971), **pages** 31–53. DOI: 10.1113/jphysiol.1971.sp009366.

[4] Huxely AF Hodgkin AL. **?**A quantitative description of membrane current and its application to conduction and excitation in nerve.**?** **in***The Journal of Physiology*: 117 (**august** 1952), **pages** 500–544. DOI: https://doi.org/10.1113/jphysiol.1952.sp004764.

[5] Min Li, Yufeng Zhou **andothers**. **?**Structural basis of TEA blockade in a model potassium channel**?** **in***Nature Structural Biology*: 10.5 (2003), **pages** 422–428. DOI: 10.1038/nsb922.

[6] Roderick MacKinnon. **?**Potassium channels and the atomic basis of selective ion conduction**?** **in***Nobel Lecture*: (2003). Available from the Nobel Prize website.

[7] D Paydafar, DB Forger **and** JC Clay. **?**Noisy Inputs and the Induction of On–Off Switching Behavior in a Neuronal Pacemaker**?** **in***Journal of Neurophysiology*: 96 (2006), **pages** 3338–3348. URL: https://doi.org/10.1152/jn.00486.2006.

[8] D Paydafar, DB Forger **and** JC Clay. *Squid Giant Axon Membrane Potential*. 2016. URL: https://doi.org/10.13026/C25C73.

[9] AL Zaninotto **andothers**. **?**Transcranial direct current stimulation (tDCS) effects on traumatic brain injury (TBI) recovery: A systematic review**?** **in***Dementia Neuropsychologia*: 13.2 (2019), 172–179. ISSN: 1980-5764. DOI: 10.1590/1980-57642018dn13-020005. URL: https://doi.org/10.1590/1980-57642018dn13-020005.

A Tables

A.1 Function prototypes of the CS model

Function type	General form	Matching CS functions
Sigmoidal	$y_0 + \frac{a}{b+e^{(c-v)/d}}$	$\tau_{A3}, \tau_{B3}, b_{2\infty}, b_{3\infty}, b_{4\infty}$
Power Sigmoidal	$y_0 + \left(\frac{a}{b+e^{(c-v)/d}}\right)^j$	$a_{2\infty}, a_{3\infty}, a_{4\infty}$
Capped Linear	$c(av + b(1-v))$ if $v \in [a, b]$	τ_{A2}
Constant	c	$\tau_{A4}, \tau_{B2}, \tau_{B4}$

Table 1: Functions in the CS model by their type. Each one offers candidate parameters for bifurcation.

A.2 Parameter values

Function	Name	Description	Value	Units
Generic	V_2	K^+ Nernst Potential	-60	mV
	g_2	K^+ Conductance	10	Ω^{-1}
	V_3	Na^+ Nernst Potential	45	mV
	g_3	Na^+ Conductance	21	Ω^{-1}
	V_4	Combined Nernst Potential	-63	mV
	g_4	Combined Conductance	10	Ω^{-1}
τ_{A2} Capped Linear	a	Lower Bound	-40	N/A
	b	Upper Bound	10	N/A
	c	Gradient	$-\frac{24}{5}$	N/A
τ_{A3} Sigmoidal	a	Scale	0.6335	N/A
	b	Ending Height	0.05426	N/A
	c	x shift	-1.932	N/A
	d	Steepness	-4.650	N/A
	y_0	y shift	1	N/A
τ_{A4}	c	Constant	12	N/A
τ_{B2}	c	Constant	50	N/A
τ_{B3} Sigmoidal	a	Scale	0.3346	N/A
	b	Ending Height	0.003225	N/A
	c	x shift	-1.9342	N/A
	d	Steepness	-4.045	N/A
	y_0	y shift	5	N/A
τ_{B4}	c	Constant	235	N/A
$a_{2\infty}$ Power Sigmoidal	a	Scale	1	N/A
	b	Ending Height	1	N/A
	c	x shift	0	N/A
	d	Steepness	-10	N/A
	j	Power	$\frac{1}{2}$	N/A
$a_{3\infty}$ Power Sigmoidal	a	Scale	1	N/A
	b	Ending Height	1	N/A
	c	x shift	-10	N/A
	d	Steepness	5	N/A
	j	Power	$\frac{1}{3}$	N/A
$a_{4\infty}$	a	Scale	1	N/A

Power Sigmoidal	b	Ending Height	1	N/A
	c	x shift	-10	N/A
	d	Steepness	20	N/A
	j	Power	$\frac{1}{4}$	N/A
$b_{2\infty}$ Sigmoidal	a	Scale	1	N/A
	b	Ending Height	1	N/A
	c	x shift	0	N/A
	d	Steepness	6	N/A
	y_0	y shift	0	N/A
$b_{3\infty}$ Sigmoidal	a	Scale	1	N/A
	b	Ending Height	1	N/A
	c	x shift	10	N/A
	d	Steepness	-5	N/A
	y_0	y shift	0	N/A
$b_{4\infty}$ Sigmoidal	a	Scale	1	N/A
	b	Ending Height	1	N/A
	c	x shift	60	N/A
	d	Steepness	-20	N/A
	y_0	y shift	0	N/A

Table 2: Initial parameter values in the CS model, with letters corresponding to the function types in subsection A.1. N/A indicates dimensionless values.